Impact of sample preparation on holographic imaging of leukocytes

Christian Klenk
Dominik Heim
Matthias Ugele
Oliver Hayden

SPIE.

Impact of sample preparation on holographic imaging of leukocytes

Christian Klenk,[†] Dominik Heim,[†] Matthias Ugele,[*] and Oliver Hayden
Technical University of Munich, Heinz-Nixdorf-Chair of Biomedical Electronics,
Department of Electrical and Computer Engineering, Munich, Germany

Abstract. The label-free analysis of leukocytes by holographic microscopy has the potential to overcome the extensive labeling procedures of conventional analysis by automated hematology analyzers and manual blood smear analysis. For the enrichment of leukocytes, selective lysis of erythrocytes is applied in flow cytometry to minimize the background. In the case of quantitative phase measurements, lysis procedures may affect the morphology of leukocytes inducing refractive index changes, which can deteriorate the specificity and sensitivity of the method. To study the effects of selective erythrocyte lysis on phase measurements of leukocytes, we compared two widespread methods: lysis by hypotonic shock followed by magnetic depletion of erythrocytes and lysis with a commercial lysis buffer containing ammonium chloride and potassium bicarbonate. We observed that lymphocytes were less affected than granulocytes and monocytes by both methods and that the intracellular changes increased with increasing incubation times. These findings indicate a significant effect of erythrocyte lysis on leukocytes and need to be studied for future hematology applications. © *The Authors. Published by SPIE under a Creative Commons Attribution 4.0 Unported License. Distribution or reproduction of this work in whole or in part requires full attribution of the original publication, including its DOI.* [DOI: 10.1117/1.OE.59.10.102403]

1 Introduction

Whole blood sample preparation plays an important role in automated hematology analysis, especially for the measurement of leukocyte concentrations, and leukocyte differential automated sample preparation allows fast and quantitative results.[1–4] However, extensive sample preparation procedures are still an issue for patient samples with interferences and can induce undesired changes in cell morphology. Automated hematology analyzers with integrated workflows have optimized preanalytics to minimize background effects and to achieve high accuracy with healthy donor samples. Flagged results often observed with patient samples require a manual review by peripheral blood smear analysis, which still remains the gold standard in hematology analysis.

Owing to its high contrast with measuring biological samples induced by different phase delays of intracellular components, digital holographic microscopy (DHM) is a label-free alternative for hematology.[5,6] In the case of leukocyte analysis, any effects on the cellular morphology caused by sample preparation procedures are critical. Intracellular refractive index changes lead to variances in quantitative phase measurements, which influence the sensitivity and specificity. Previous work focusing on the label-free holographic analysis of leukocytes analyzed either cells isolated by Ficoll density centrifugation or cells in culture.[7–13] Central laboratory applications require integrated workflows for a high-throughput analysis. The selective lysis of erythrocytes provides a rapid method for the isolation of leukocytes from whole blood and is widely used in commercial hematology analyzers and fluorescence flow cytometers. Recently, we demonstrated that a selective lysis of erythrocytes by hypotonic shock is suitable for a rapid detection and differentiation of leukemic diseases by DHM.[14] Unfortunately, this working step still requires

---

*Address all correspondence to Matthias Ugele, E-mail: matthias.ugele@tum.de

[†]Both authors contributed equally to this manuscript

a depletion of remaining erythrocyte fragments to reduce background artifacts in the images, which is a costly and time-consuming procedure. Commercial erythrocyte lysis buffers containing ammonium chloride and potassium bicarbonate provide an alternative for complete lysis of erythrocytes without further preanalytical steps. So far, the impact of these lysis buffers has only been studied for the change of flow cytometry parameters, such as fluorescence intensities.[15] The impact on cellular refractive index changes and, therefore, on the phase contrast analyzed by DHM has not been studied.

To address this problem, we compared the effects of erythrocyte lysis on DHM imaging of leukocytes. We applied two different lysis methods: erythrocyte lysis by a commercial lysis buffer containing ammonium chloride and potassium bicarbonate and our previously established method of selective lysis by hypotonic shock followed by immunomagnetic depletion. In addition, we analyzed the effects of the lysis buffer incubation times on cell morphologies and intracellular phase contrast changes. It could be shown that different sample preparation methods (SPMs) have a significant effect on leukocyte measurements with DHM. Especially granulocytes and monocytes appear to be more sensitive to erythrocyte lysis methods, while for lymphocytes the observed impact was smaller. Finally, even incubation times of the lysis buffer have a major influence on leukocyte measurements by DHM.

2 Methods

2.1 Digital Holographic Microscopy

Measurements were performed with a transmission off-axis holographic microscope provided by Ovizio Imaging Systems, Belgium, which has been described before.[14,16] It is a double-differential DHM and is equipped with a 40× NA 0.55 Nikon CFI LWD 40× Cremove objective, a 528-nm Oslon PowerStar SLED (Osram), and a PointGrey Grashopper GS3U332S4 camera (105 fps, exposure time 5 μs) for high-throughput imaging (Fig. 4, Appendix A). By using a low-coherent light source instead of a coherent laser, the image degradation is eliminated and the image quality is improved.[17,18] The light beam emitted from the light-emitting diode first passes a Köhler illumination path and then passes through the sample, which is located in the back focal plane of the microscope objective (Fig. 6, Appendix A). Either a blazed or Ronchi diffraction grating is used to split the incident beam into a diffracted (reference beam) and a nondiffracted beam (object beam). A lens located at focal distance of the grating allows a reshaping of both beams in parallel orientation. A wedge at the optical path of the reference beams induces a small shift of the images produced by diffracted and nondiffracted beams in order to obtain differential interferogram, as described in detail by Dubois and Yourassowsky.[19] In parallel to the wedge, compensation means are introduced in the optical path of the nondiffracted light beam compensating the phase shift introduced by the wedge in the diffracted beam. In a last step, the object and reference beam are focused on a detector, resulting in an interferogram. A detailed description of the working principle and microscope setup is described by Dubois and Yourassowsky.[19,20] Reconstruction of the phase and amplitude images out of the holograms were performed using the OsOne Software Version 5.1 (Ovizio Imaging Systems, Belgium).

2.2 Microfluidics

A channel with a height of 50 μm, a width of 500 μm, and a total length of 50,000 μm was used for precise alignment of a submonolayer of blood cells. The microfluidic poly(methyl methacrylate) (PMMA) system (Fraunhofer ICT-IMM, Mainz) contained five inlets with a top and bottom flows (z-sheaths), two side flows (x and y sheaths), and one sample flow. The samples were diluted in 0.9% polyvinylpyrrolidone (PVP, molecular weight $M_w = 1.3$MD, Alfa Aesar) in phosphate-buffered saline (PBS). Sheath flow conditions were established using PBS as a sheath flow buffer. A total flow rate of 1 μl^{-1} was adjusted by the neMESYS Base 120 pump system with five modules (cetoni GmbH). Each slot was equipped with a 2.5-ml gas tight syringe (VWR). During the measurements, all pumps were adjusted to a flow rate of 0.2 μl^{-1}. Microfluidic components (tubes, connections) and a six-port injection valve (V-451 six-port medium pressure injection valves bulkhead version .040 Black) were purchased from IDEX

Health & Science. Maximum Reynolds numbers in the single digit range (Re ≈ 4.1) have been calculated for the measurement state. Therefore, measurements were performed in the laminar flow regime.[21]

2.3 Data Processing

Data processing and analysis of leukocyte data were performed as described by Ugele et al.[14] In short, floating point phase-shift pixel values for each recorded phase image within the interval of [0,8] were converted to grayscale values. By calculating the median gray value from the first 11 images of the resulting grayscale image, a background image was determined. By subtracting this background image from each phase image, a correction of the background and, therefore, a reduction of the background noise was achieved. For each corrected image, a binary picture was generated by thresholding at the gray level of 28. This resulted in a removal of holes in binary images. As every image contained more than one cell, all objects were segmented. For each object, parameters based on the phase values inside the contour and based on a gray-level co-occurrence matrix[22] were calculated. Gating strategies for the differentiation of leukocytes were developed in Kaluza flow cytometry analysis (v.2.1, Beckman Coulter).

2.4 Sample Preparation

Leukocytes were isolated from the healthy donors by two different preanalytical methods. All human samples were collected from volunteers with informed consent.

2.4.1 Erythrocyte lysis using hypotonic shock followed by erythrocyte depletion (sample preparation method 1)

Leukocytes were isolated from ethylenediamine tetra-acetic acid (EDTA) coagulation-inhibited peripheral blood by selective hypotonic water lysis of erythrocytes, as described elsewhere.[15] For all samples, 1-ml blood was processed. To remove remaining erythrocyte fragments, the Miltenyi Biotec MACSxpress Erythrocyte Depletion Kit was used. After centrifugation (400 g for 10 min) the remaining pellet was resuspended in 500-μl 0.9% PVP solution. An average time from blood drawing to imaging of 3 to 4 h was met.

2.4.2 Erythrocyte lysis by lysis buffer (sample preparation method 2)

A conventional erythrocyte lysis buffer (J62990 RBC lysis buffer for human, Alfa Aesar, Haverhill, Massachusetts) was used for the lysis of human erythrocytes. This ammonium chloride- and potassium bicarbonate-based buffers are used for the isolation of deoxyribonucleic acid and ribonucleic acid, as well as for several flow cytometer assays.[23,24] About 1 ml of EDTA coagulation-inhibited peripheral blood was mixed with 4 ml of the lysis buffer at room temperature and incubated for 5, 10, 15, 20, and 25 min with continuous mixing on a roller mixer. After centrifugation at 1000 g for 10 min to diminish the amount of debris, the remaining pellet was resuspended in 500-μl 0.9% PVP solution.

2.4.3 Flow cytometry measurements of leukocytes

Leukocytes were isolated using SMP 2. Cells were fluorescently labeled with anti-CD45-VioBlue and anti-CD14-FITC to enable subtyping of leukocytes. Staining with anti-CD45 allowed a differentiation between leukocytes and debris, whereas anti-CD14 allowed a discrimination of monocytes and lymphocytes. All other leukocyte subtypes were removed by gating in the forward and side scatter plots. To exclude a possible activation of cells by SPM 2, leukocytes were isolated, as described in Sec. 2.4.2, and fluorescently labeled with anti-CD45-VioBlue and anti-CD71-FITC or with anti-CD45-VioBlue, anti-CD54-FITC, and anti-CD64-PE (Fig. 5, Appendix A).[25–27] Flow cytometry measurements were performed using an MACSQuant Analyzer 10 (Miltenyi Biotec GmbH). For each incubation time, three measurements were performed.

3 Results and Discussion

3.1 *Comparison of Sample Preparations Methods*

To determine the effects of sample preparation on leukocytes, the two parameters, namely, "optical phase delay maximum" (OPDM, maximal phase delay value of the segmented object) and "equivalent diameter" (ED, mean diameter of cell contour area), were investigated (Fig. 1), because changes in these parameters represent changes in the outer and/or inner shape of the cells. OPDM and ED of leukocyte raw data were plotted against the different SPMs, SPM 1 [Fig. 1(a)] and for each application time of SPM 2 [Figs. 1(b)–1(e)]. Initially, four main
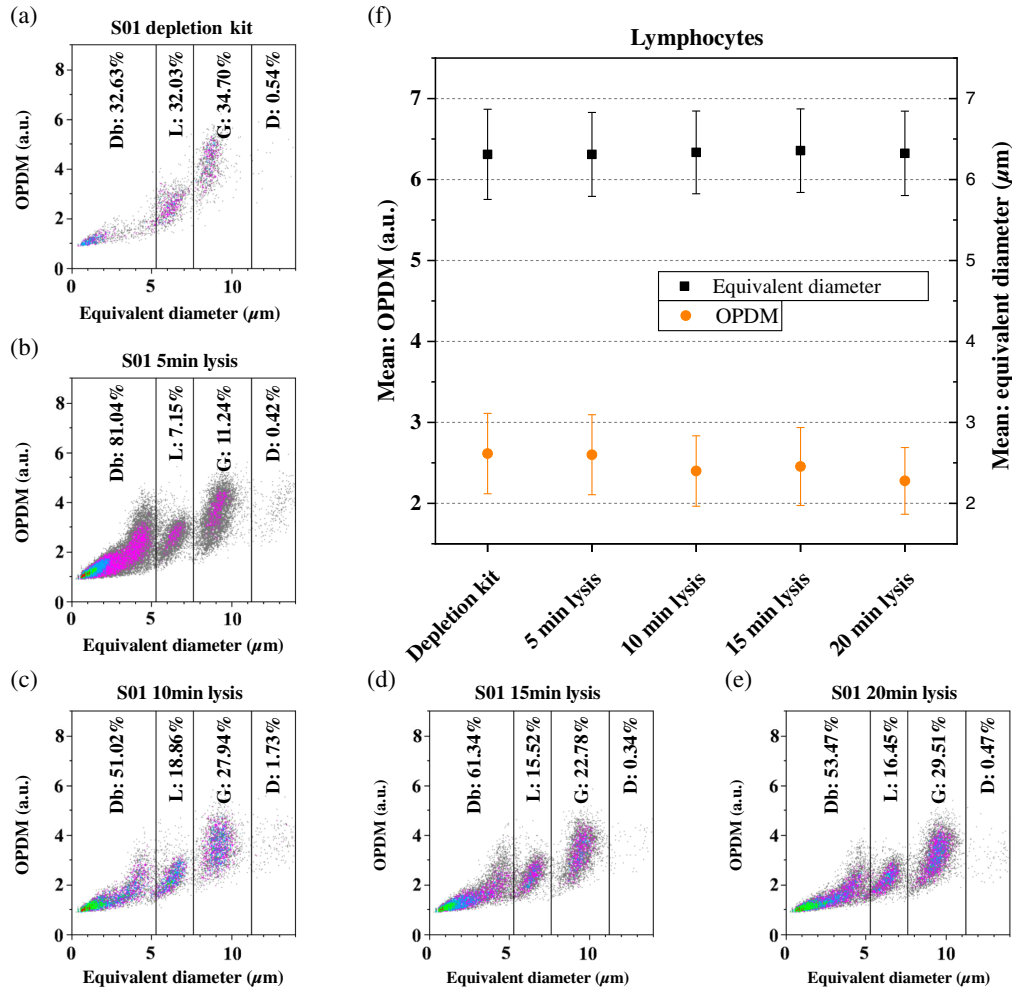

Fig. 1 Influence of lysis buffer incubation time on the amount of cell debris and lymphocytes: (a) label-free density plots of leukocytes purified by hypotonic shock followed by magnetic depletion of erythrocytes. (b)–(e) Label-free density plots of leukocytes purified by erythrocyte lysis with the commercial lysis buffer with incubation times of (b) 5 min, (c) 10 min, (d) 15 min, and (e) 20 min. The plots (a)–(e) are divided into four sections indicating cell debris (Db), lymphocytes (L), granulocytes and monocytes (G), and duplets (D). The use of hypotonic shock followed by magnetic depletion of erythrocytes resulted in the lowest amount of cell debris, with greater 5-min incubation time of the lysis buffer significantly reducing the amount of cell debris. Parameters ED and OPDM are plotted. Each density plot shows representative single-cell data from one sample. Percentages of cells are indicated for each gate. (f) The changes in the parameters ED and OPDM of lymphocytes [gate L in (a)–(e)] for the different SPMs, respectively, incubation times are plotted. Overall, only slight changes were observed, indicating that lymphocytes are not affected by different treatment. Data points show the pooled data from two samples. Error bars represent the first standard deviation of the grouped population.

populations, consisting of cell debris, lymphocytes, granulocytes and monocytes, and aggregates were separated by gating [Figs. 1(a)–1(e)]. First, the amount of cell debris between SPM 1 and SPM 2 was compared. By the use of SPM 1, about 32% of cell debris occurred, which is significantly lower than SPM 2. This can be explained by the use of the erythrocyte depletion kit, which removed a high amount of the remaining erythrocyte fragments. However, the magnetic depletion is costly and time-consuming (5 min incubation time, 10 min magnetic separation, 10 min centrifugation) and, therefore, SPM 1 does not provide a suitable solution for a low-cost application at the point of care. In contrast, a high amount of 81% of cell debris for 5-min application time of SPM 2 was observed. With increased incubation time, a reduction to 51% (10 min), 61% (15 min), and 53% (20 min) was detected. This observation was confirmed by the reduction of cell debris from 85% (5 min) to 40% (10 min), 71% (15 min), and 35% (20 min) in a second measured sample. A higher amount of cell debris at 15 min than at 10 and 20 min occurred in both samples, which was quite unexpected. Nevertheless, the overall observation that an incubation time longer than 5 min is necessary to effectively reduce cell debris was confirmed. Furthermore, the total number of measured leukocytes was significantly higher for SPM 2. With SPM 2, nearly 3.8 as much cells as with SPM 1 were acquired (1870 cells on average for SPM 1 and 7126 cell on average for SPM 2). It seems likely that the magnetic depletion of erythrocytes leads to cell loss, due to sedimentation effects and physical interactions of leukocytes with erythrocyte–magnetic bead complexes induced by the high amount of added magnetic beads (600 μl for 1 ml blood) to ensure efficient depletion. Consequently, if samples with low leukocyte numbers are analyzed, SPM 2 should be favored.

To determine the qualitative impact of sample preparation on leukocytes, the populations of lymphocytes (gate L) and granulocytes and monocytes (gate G) were evaluated. For each, OPDM and ED of the grouped populations of two samples from different donors were plotted against the applied method [Figs. 1(f) and 2(f)]. For lymphocytes, no significant change in OPDM and ED was observed, while the granulocyte and monocyte population showed a clear tendency of decreasing OPDM and increasing ED with increased SPM 2 application time compared to SPM 1. To better analyze the changes in inner and outer cell shapes, the granulocyte and monocyte population was divided into four sections [a1 to a4, Figs. 2(a)–2(e)]. Initially, a shift in the percentage of each section toward lower OPDM was observed, when comparing SPM 1 and SPM 2. Most important, the percentage of cells in gate a1 was significantly reduced from about 16% in SPM 1 to below 2% in SPM 2. With increased incubation time of SPM 2, the percentage of cells in a1 decreased from 1.7% (5 min) to about 0.1% (15 and 20 min). The amount of cells in gate a2 decreased from 50.8% to 23.0%, and the percentage of cells in gates a3 and a4 increased from 45.6% to 65.1% and 1.8% to 11.8%, respectively. These changes in the gates a1 to a4 confirmed the previously observed changes to lower OPDM with increased incubation time of SPM 2.

As discussed above, more than 5 min incubation time of SPM 2 should be applied to avoid high amounts of cell debris. However, increasing incubation time seems to affect the leukocytes more strongly. An uptake of lysis buffer inside the cells and an efflux of intracellular components could possibly be the reason for the increase in ED and the decrease in OPDM in granulocytes and monocytes over time. An explanation why lymphocytes were less affected could be the higher ratio of nucleus to plasma in the cells, which limits an uptake of lysis buffer. On the contrary, with a smaller ratio of nucleus to plasma, granulocytes and monocytes were more affected, as a higher uptake of lysis buffer might lead to swelling of cells and, therefore, to increased ED and decreased OPDM. To confirm these findings, more samples should be measured, including the analysis of other parameters describing the inner consistency, such as contrast, refractive index, or dry mass. Furthermore, the impact of the sample preparation on leukocyte differentiation should be analyzed to guarantee a reliable classification of leukocytes, as described before.[14] These experiments will be addressed by planned future studies.

3.2 Impact of Lysis Buffer Incubation Time on Leukocyte Subpopulations

Finally, the impact of SPM 2 on leukocyte subpopulations was investigated by multicolor fluorescence flow cytometry. It was of special interest, if an increased incubation time of the lysis
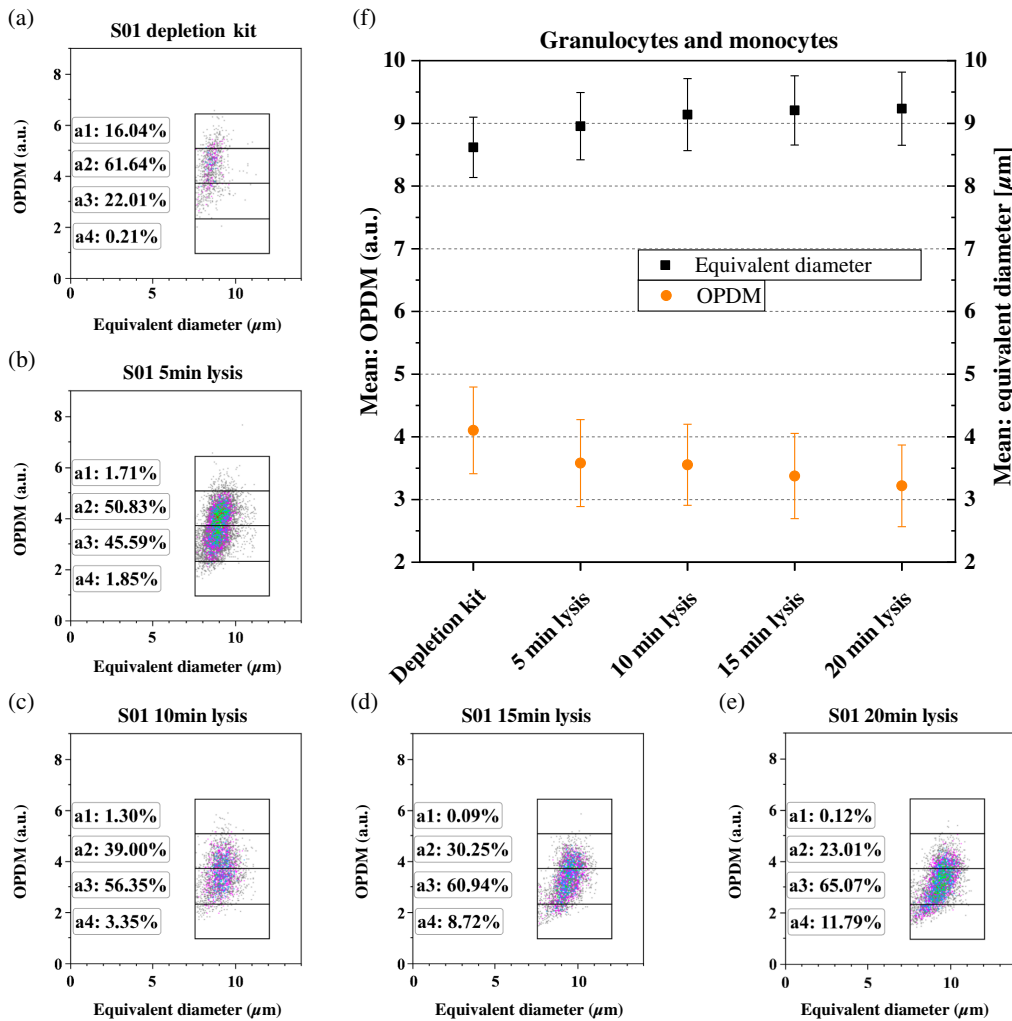
Fig. 2 Influence of lysis buffer incubation time on granulocytes and monocytes: (a) label-free density plots of granulocytes and monocytes purified by hypotonic shock followed by magnetic depletion of erythrocytes. Only cells from gate G in Fig. 1 are shown. (b)–(e) Label-free density plots of granulocytes and monocytes purified by lysis of erythrocytes by the use of lysis buffer with incubation times of (b) 5 min, (c) 10 min, (d) 15 min, and (e) 20 min. Only cells from gate G in Fig. 1 are shown. The plots (a)–(e) are divided into four sections a1, a2, a3, and a4. In comparison to (a) a shift to lower percentage of cells in gate a1 was observed in (b)–(e). With increased incubation time, a shift to a higher amount of cells in gates a3 and a4 and a shift to a lower amount of cells in gate a2 were observed. Parameters ED and OPDM are plotted. Each density plot shows representative single-cell data from one sample. Percentages of cells are indicated for each gate. (f) The changes in the parameters ED and OPDM of granulocytes and monocytes (gate G in Fig. 1) for the different SPMs, respectively, incubation times are plotted.

buffer would induce cell loss. This could be directly observed by a change in the relative amount of lymphocytes, granulocytes, and monocytes. Therefore, leukocytes were isolated and labeled as described in Sec. 2. Three blood samples of one healthy donor were independently labeled and each measured one time. As a reference, the leukocyte differential of the Sysmex XN-350 hematology analyzer was used. Granulocytes between 55.1% and 57.9%, lymphocytes between 39.1% and 41.2% and monocytes between 2.9% and 3.8% were determined by flow cytometry (Fig. 3), which are in good agreement with the results from the Sysmex XN-350 (56.2% granulocytes, 38.2% lymphocytes, and 5.6% monocytes). The observed differences of up to 4% between flow cytometry and Sysmex XN-350 measurements are most likely due to the different methods used for leukocyte isolation (SPM 2 for flow cytometry, fully
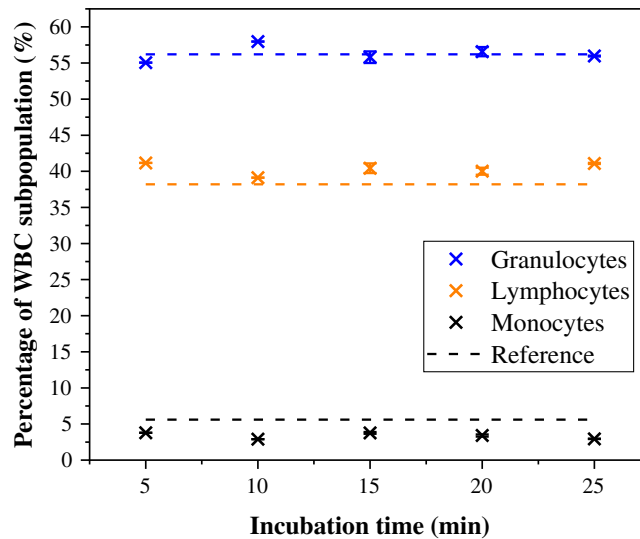
Fig. 3 Impact of lysis buffer incubation times on leukocytes subpopulations: flow cytometry measurements of one sample for five different lysis buffer incubation times are plotted. By labeling the leukocytes subpopulations with fluorescent markers, the relative concentrations of monocytes, lymphocytes, and granulocytes were determined. Reference measurements of leukocyte subpopulations in whole blood were performed with the Sysmex XN-350 (dashed lines). Each data point shows average values of three measurements. All samples were from one healthy donor and were labeled independently from the others.

automated lysis and staining of cells by the Sysmex XN-350). Incubation times up to 25 min of SPM 2 did not significantly influence the relative percentage of the different subpopulations, which show the reliability and applicability of the applied leukocyte preparation method also for DHM. Nevertheless, cell loss might occur in SPM 2, but the obtained results strongly indicate that the loss of cells occurs equally distributed across all leukocyte subpopulations.

4 Conclusion

Taken together, a significant impact of different SPMs on quantitative phase measurements of leukocytes was shown. Changes in the inner and outer shapes of leukocytes were induced by SPM 2, which might possibly also affect a label-free leukocyte differential by DHM. For this reason, further studies have to be performed to intensively analyze possible effects and verify that SPM 2 can also be used for leukocyte analysis instead of SPM 1. To minimize changes in OPDM and ED the incubation time of SPM 2 should be as short as possible. However, an acceptable amount of cell debris for imaging has to be achieved and, therefore, we suggest a 10-min incubation time of the lysis buffer as optimal trade-off of reduced cell debris and impact on leukocytes. In addition, the overall yield of leukocytes was 3.8 times higher by the use of the lysis buffer, which allows also an applicability for clinical samples with extremely low leukocyte numbers. In conclusion, selective lysis of erythrocytes by the use of lysis buffers containing ammonium chloride and potassium bicarbonate provides a suitable alternative to selective lysis by hypotonic shock, as long as effects on leukocytes are carefully considered.

5 Appendix A: Supplements

Figure 4 depicts an overview of the holographic setup and microfluidic principle. Figure 5 shows activation measurements of leukocytes before and after DHM measurements. Overview of the used DHM principle (Fig. 6). Exemplary phase maps of leukocytes isolated with SPM 1 and SPM 2 (Fig. 7). Segmentation of phase images (Fig. 8).
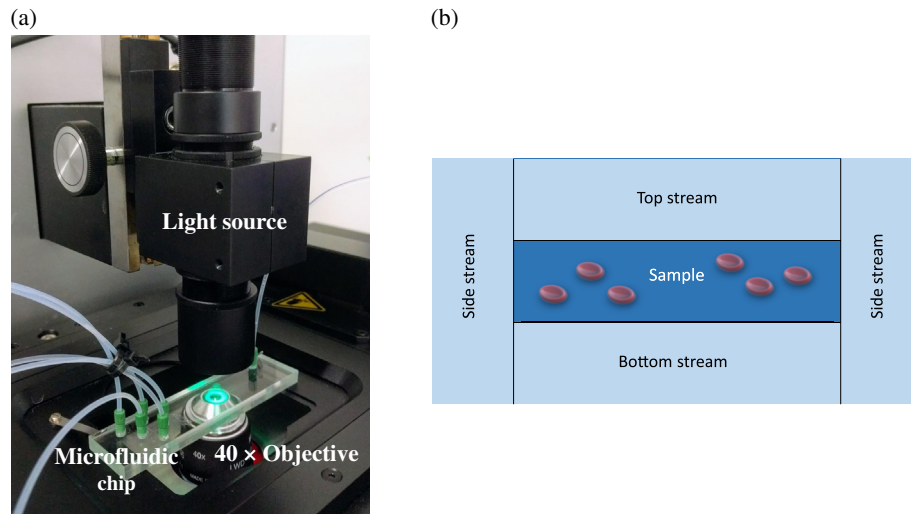
(a)

(b)

Fig. 4 Microfluidic and optical setup for the measurement of leukocytes: (a) differential DHM for high-throughput imaging (105 fps) of blood cells using a 40× NA 0.55 objective and a 528-nm SLED Koehler illumination light source. A PMMA microfluidic channel with one outlet and five inlets was used for the alignment of cells and high-throughput sample presentation. (b) Schematic representation of the sheath and sample flows of the channel cross section.
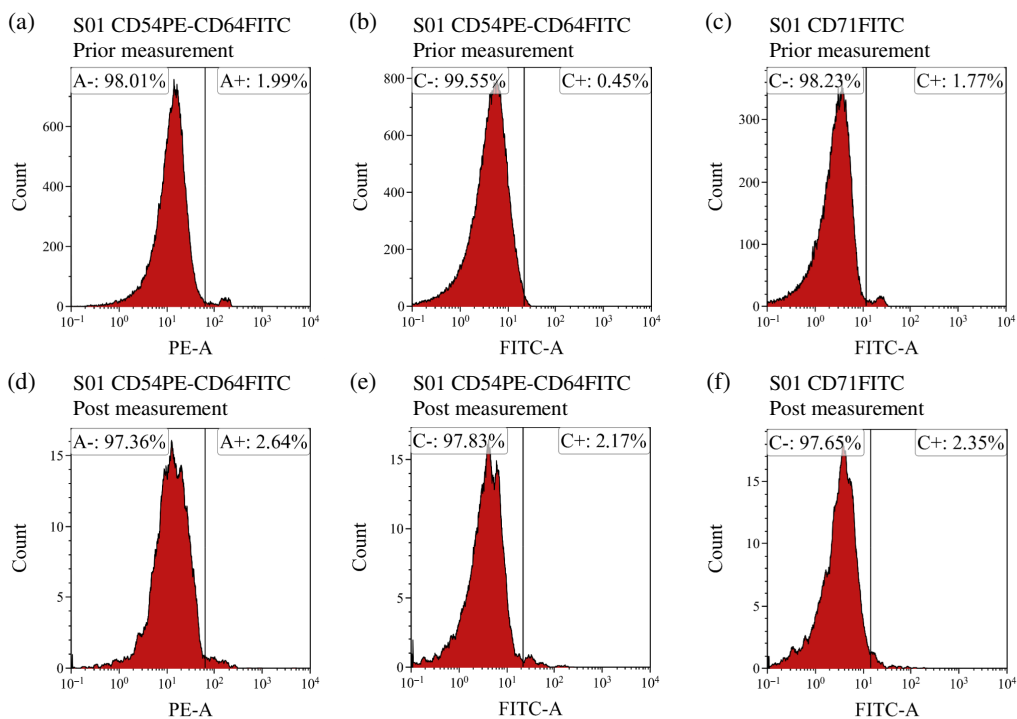

Fig. 5 Influence of sample preparation and DHM measurement on leukocytes: activation measurement of white blood cells (a)–(c) directly after sample preparation and (d)–(f) directly after DHM measurement. Leukocytes were fluorescently labeled with (c) and (f) anti-CD45-VioBlue and anti-CD71-FITC or (a), (b), (d), and (e) with anti-CD45-VioBlue, anti-CD54-FITC and anti-CD64-PE. The measurements were performed using an MACSQuant Analyzer 10. Each subfigure shows representative measurements of one sample. No significant activation of cells (gate A+ or C+) was observed.
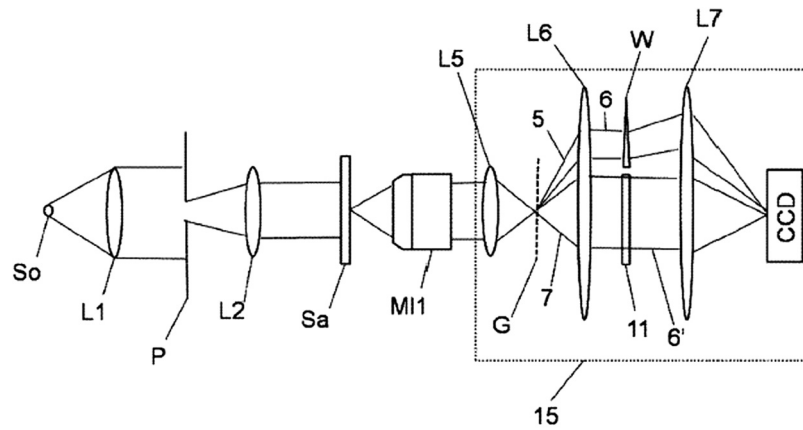
Fig. 6 Optical setup of the differential DHM. The light beam emitted by a partially coherent 528-nm SLED light source (So) passes a Köhler illumination path and then passes through the sample (Sa), which is located in the back focal plane of the microscope objective (MI1). The beam is then split by a diffraction grating (G) into a diffracted (reference beam) and a non-diffracted part (object beam). The diffracted beam passes a compensating means (11), whereas the nondiffracted beam passes a wedge (W). Finally, both beams are focused on an imaging device where the hologram can be observed. L1, L2, L5, L6, and L7, lenses; P, pinhole; 5, diffracted light beam; 6, nonzero-order diffracted parallel light beam; 7, nondiffracted light beam; 6′, zero-order diffracted parallel light beam; 15, interferometer. Image adopted from Ref. 20.
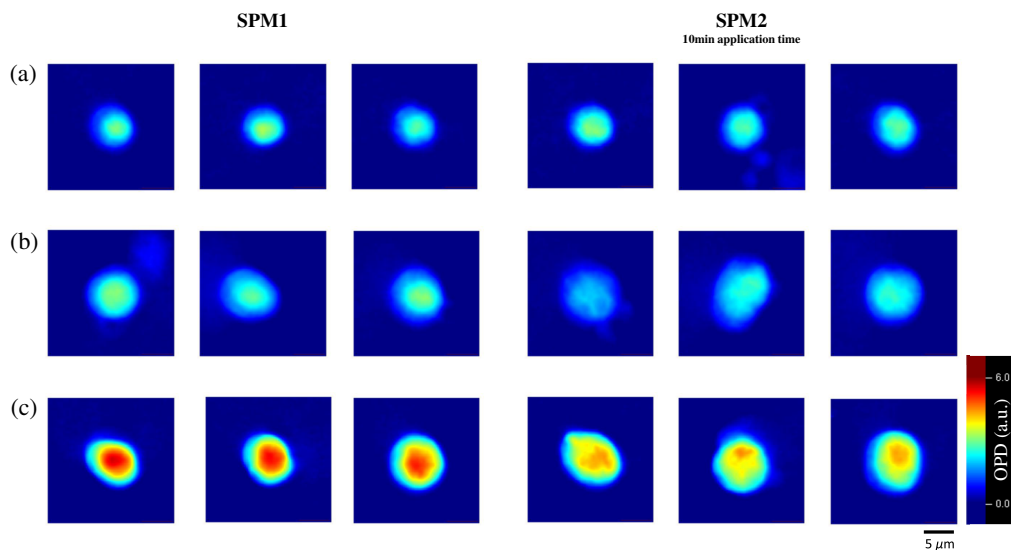

Fig. 7 Exemplary false color phase images of three leukocyte subpopulations. (a) Lymphocyte phase images show low difference between SPM 1 and SPM 2. (b) The OPDM of monocytes is higher in SPM 1 than in SPM 2. This effect is even more distinct for (c) granulocytes. SPM 2 with 10-min incubation time. Scale bar is 5 μm.
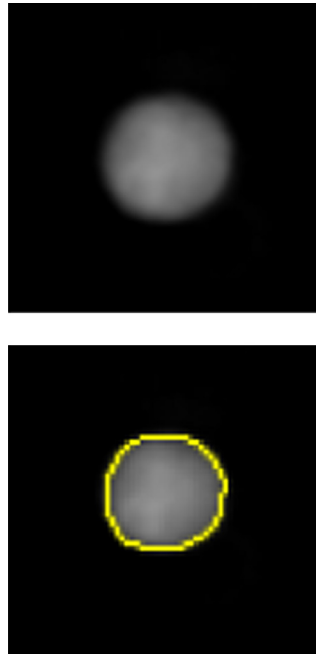
Fig. 8 Segmentation of leukocyte phase images. Leukocytes were segmented by common thresholding segmentation techniques before the calculation of cellular parameters based on their morphology and phase delay.

Acknowledgments

References

1. L. Meintker et al., "Comparison of automated differential blood cell counts from Abbott Sapphire, Siemens ADVIA 120, Beckman Coulter DxH 800, and Sysmex XE-2100 in normal and pathologic samples," *Am. J. Clin. Pathol.* **139**, 641–650 (2013).
2. S. H. Kang et al., "Comparison of four hematology analyzers, CELL-DYN Sapphire, ADVIA 120, Coulter LH 750, and Sysmex XE-2100, in terms of clinical usefulness," *Int. J. Lab. Hematol.* **30**, 480–486 (2008).
3. M. Bruegel et al., "Comparison of five automated hematology analyzers in a university hospital setting: Abbott CELL-DYN Sapphire, Beckman Coulter DxH 800, Siemens ADVIA 2120i, Sysmex XE-5000, and Sysmex XN-2000," *Clin. Chem. Lab. Med.* **53**, 1057–1071 (2015).
4. P. O. Rabinovitch et al., "Validation, verification, and quality assurance of automated hematology analyzers," Proposed Standard, 2nd ed., Vol. 30 (2010).
5. M. K. Kim, "Principles and techniques of digital holographic microscopy," *SPIE Rev.* **1**(1), 018005 (2010).
6. Y. K. Park, C. Depeursinge, and G. Popescu, "Quantitative phase imaging in biomedicine," *Nat. Photonics* **12**(10), 578–589 (2018).
7. Y. Li et al., "Accurate label-free 3-part leukocyte recognition with single cell lens-free imaging flow cytometry," *Comput. Biol. Med.* **96**, 147–156 (2018).
8. D. Vercruysse et al., "Three-part differential of unlabeled leukocytes with a compact lens-free imaging flow cytometer," *Lab Chip* **15**, 1123–1132 (2015).
9. J. Yoon et al., "Label-free characterization of white blood cells by measuring 3D refractive index maps," *Biomed. Opt. Express* **6**, 3865 (2015).
10. J. Yoon et al., "Identification of non-activated lymphocytes using three-dimensional refractive index tomography and machine learning," *Sci. Rep.* **7**(1), 1–10 (2017).

11. J. Persson et al., "Cell motility studies using digital holographic microscopy," in *Microscopy, Science, Technology, Applications and Education*, pp. 1063–1072 (2010).

12. N. McReynolds et al., "Multimodal discrimination of immune cells using a combination of Raman spectroscopy and digital holographic microscopy," *Sci. Rep.* **7**, 1–11 (2017).

13. G. Stybayeva et al., "Lensfree holographic imaging of antibody microarrays for high-throughput detection of leukocyte numbers and function," *Anal. Chem.* **82**(9), 3736–3744 (2010).

14. M. Ugele et al., "Label-free high-throughput leukemia detection by holographic microscopy," *Adv. Sci.* **5**(12), 1800761 (2018).

15. J. Vuorte, S. E. Jansson, and H. Repo, "Evaluation of red blood cell lysing solutions in the study of neutrophil oxidative burst by the DCFH assay," *Cytometry* **43**(4), 290–296 (2001).

16. M. Ugele et al., "Label-free, high-throughput detection of P. falciparum infection in sphered erythrocytes with digital holographic microscopy," *Lab Chip* **18**, 1704–1712 (2018).

17. F. Dubois et al., "Partial spatial coherence effects in digital holographic microscopy with a laser source," *Appl. Opt.* **43**, 1131–1139 (2004).

18. J. Dohet-Eraly et al., "Quantitative assessment of noise reduction with partial spatial coherence illumination in digital holographic microscopy," *Opt. Lett.* **41**, 111–114 (2016).

19. F. Dubois and C. Yourassowsky, "Digital holographic microscope for 3D imaging and process using it," US Patent 7, 362.449 B2, pp. 1–18 (2004).

20. F. Dubois and C. Yourassowsky, "Off-axis interferoemter," US Patent 9, 207, 638 B2, pp. 1–15 (2015).

21. H. Bruus, *Theoretical Microfluidics*, Oxford Master Series in Physics, Vol. **18**, pp. 40–41, Oxford University Press, Oxford (2007).

22. R. Haralick, K. Shanmugam, and I. Dinstein, "Textural features for image classification," *IEEE Trans. Syst. Man Cybern.* **SMC3**, 610–621 (1973).

23. M. A. Boyd et al., "Adaptation of red blood cell lysis represents a fundamental breakthrough that improves the sensitivity of Salmonella detection in blood," *J. Appl. Microbiol.* **118**, 1199–1209 (2015).

24. X. Bossuyt, G. E. Marti, and T. A. Fleisher, "Comparative analysis of whole blood lysis methods for flow cytometry," *Commun. Clin. Cytom.* **30**(3), 124–133 (1997).

25. C. M. Herra, C. T. Keane, and A. Whelan, "Increased expression of Fcγ receptors on neutrophils and monocytes may reflect ongoing bacterial infection," *J. Med. Microbiol.* **44**(1996), 135–140 (1996).

26. M. Motamedi, L. Xu, and S. Elahi, "Correlation of transferrin receptor (CD71) with Ki67 expression on stimulated human and mouse T cells: the kinetics of expression of T cell activation markers," *J. Immunol. Methods* **437**, 43–52 (2016).

27. G. Stent et al., "The kinetics of surface expression of CD11/CD18 integrins and CD54 on monocytes and macrophages," *Clin. Exp. Immunol.* **100**(2), 366–376 (1995).

Christian Klenk is a doctorate student at the Technical University of Munich (TUM). He received his MSc degree in electrical and computer engineering from TUM in 2018. His current research interests are in the field of digital holography and microfluidics.

Dominik Heim is a medical doctorate student and studies medicine and biophysics at TUM.

Matthias Ugele received his BSc and MSc degrees in biochemistry and biology from the University of Regensburg, Germany, in 2012 and 2015, respectively, and his Dr.-Ing. degree in 2018 from the Friedrich-Alexander University Erlangen-Nürnberg. Currently, he is a post-doctoral group leader at the Heinz-Nixdorf chair of Biomedical Electronics at TUM.

Oliver Hayden completed his doctorate in 1999 at the University of Vienna. After holding a postdoctoral position at Harvard University, he joined the IBM Research Laboratory in Zürich in 2005. Since 2007, he has been researching organic electronic techniques and *in-vitro* diagnosis of blood cells at Siemens Corporate Technology and Siemens Healthcare. In 2017, he was appointed to the Heinz-Nixdorf-Chair for Biomedical Electronics at TUM.